Nanofibrils from oil palm trunk: effect of delignification and fibrillation technique

Lukmanul Hakim Zaini[1,2]* , Wolfgang Gindl-Altmutter[1], Claudia Gusenbauer[1], Istie Sekartining Rahayu[2], Muhammad Adly Rahandi Lubis[3], Andreas Mautner[4,5] and Stefan Veigel[1]

Abstract

Oil palm trunk (OPT) is an inexpensive, abundantly available by-product of palm oil production which is typically not put to material use. Due to its comparably high cellulose content, OPT represents a suitable raw material for the preparation of cellulose nanofibrils (CNFs). Aiming for full utilization of the raw material and minimized energy demand, non-delignified and partially delignified (alkali-pretreated) OPT was subjected to mechanical fibrillation in the present study. As compared to CNFs from fully delignified OPT, the lignin-rich microfibrils obtained by this approach generally showed higher average fibril diameters, lower thermal stability as well as lower viscosity, and higher sedimentation rate in suspension. However, the combination of alkali-pretreatment and fibrillation by disc-grinding and subsequent high-pressure homogenization resulted in fibrils with properties similar to those of CNFs from fully delignified OPT. As proven by IR-spectroscopy, thermogravimetry and chemical composition analysis, alkali-treated OPT fibrils still contained substantial amounts of residual lignin which could, for instance, act as a natural coupling agent or binder in composite applications. Moreover, the facile delignification process applied herein requires far less chemicals and energy than conventional pulping and is thus beneficial from both the economic and ecological perspective.

Keywords By-product, Delignification, Fibrillation, Nanofibrils, Oil palm trunk

Introduction

In industrial palm oil production, substantial amounts of oil palm trunk (OPT) arise as a by-product after the final stage of the plantation life cycle (25–30 years). OPT production in Indonesia is expected to reach 59 million tons in 2030 [1]. Meanwhile, Malaysia is well-known as the largest producer of palm oil (51% of global production), with 86 million metric tons of oil palm trees (*Elaeis guineensis* Jacq.) produced annually [2, 3]. The price of each trunk is estimated at about USD 7–10, which is low in terms of raw material price since cutting-down costs are known to be high [4, 5]. The remaining trunks are mostly left in the field as compost, or serve as unintended breeding places for insect pests and white rot fungi, or are set on fire leading to rising greenhouse gas levels [4, 6]. The transformation of OPT into value-added products such as, e.g., panel-type materials is thus highly practical from both an economic and ecological perspective [7]. In such applications, typically only the outer part of the trunk is used while the inner part, mainly consisting of soft parenchyma tissue, is left unused [8]. While wood is primarily made up of fiber cells, OPT consists of two main structural components,

*Correspondence:
Lukmanul Hakim Zaini
lukmanhz@apps.ipb.ac.id
[1] Institute of Wood Technology and Renewable Materials, Department of Material Sciences and Process Engineering, University of Natural Resources and Life Sciences, Vienna (BOKU), Vienna, Austria
[2] Department of Forest Products, Faculty of Forestry and Environment, IPB University, Bogor, Indonesia
[3] Research Center for Biomass and Bioproducts, National Research and Innovation Agency, Cibinong, Indonesia
[4] Institute of Materials Chemistry, Faculty of Chemistry, University of Vienna, Vienna, Austria
[5] Institute of Environmental Biotechnology, IFA-Tulln, University of Natural Resources and Life Sciences, Vienna (BOKU), Vienna, Austria

Zaini *et al. Journal of Wood Science*   (2024) 70:19

Page 2 of 16

i.e., parenchyma tissue and vascular bundles. The outer part of the trunk is dominated by vascular bundles (51%), whereas parenchyma tissue prevails in the center (70%) [5]. The vascular bundles are compact, fibrous, and less hygroscopic, while the parenchyma cells are soft, spongy, and extremely hygroscopic [6, 9]. The parenchymatous ground tissue is composed of thin-walled spherical cells which can easily be separated by mechanical means (e.g., grinding). Moreover, the thin walls of parenchyma cells fibrillate easily which is particularly true for the non-lignified cell walls from the upper part of the trunk [5].

Aside from morphological differences, wood and non-wood biomass also differ in their biochemical composition. In general, wood contains more lignin than herbaceous and agricultural biomass, with hard- and softwood containing 18–25% and 25–35% lignin, respectively [10]. For most wood species, the hemicellulose content is around 20–30% and the cellulose content is 40–45% of the dry substance [11]. In comparison, OPT contains around 18–23% lignin, 12–17% hemicellulose, and 38–41% cellulose [12–16]. Thus, OPT contains almost the same amount of cellulose as wood but OPT cell walls might be expected to fibrillate easier due to their lower thickness and lignin content. These properties make OPT a potential source for the preparation of cellulose nanofibers, commonly referred to as nanocellulose (NC). Its unique properties (e.g., rheological properties, high strength and stiffness, transparency, barrier properties, etc.) allow NC to be used in a plethora of application areas including papermaking, polymer reinforcement, packaging, cosmetics, pharmaceuticals, and electronics. The term cellulose nanofibrils (CNFs) denotes high L/D-ratio nanofibrils extracted from any cellulose source (typically wood) by mechanical fibrillation methods such as micro-grinding, high-pressure homogenization, microfluidization, or cryo-crushing. In order to weaken the structural integrity of the starting material and facilitate the liberation of individual fibrils from the cell wall, chemical delignification and, optionally, further physical, chemical, or enzymatic pretreatment steps are usually applied prior to defibrillation. For the common starting material wood, delignification and pretreatment result in low efficiency of fibrillation as well as substantial consumption of chemicals and energy. In this regard, OPT potentially offers a significant advantage over wood since its lower lignin content and thin cell walls allow for individualization into CNFs with significantly lower demand for chemicals and energy.

In a number of publications (e.g., [17–19]), OPT has been used as a starting material for the preparation of cellulose nanofibers. Luo, Wang [20] left bleached OPT fibers to soak in NaOH/urea solution and mechanically fibrillated the fully swollen fibers to obtain OPT nanofibers. The latter showed a diameter in the range of 10–100 nm and a length varying from hundreds of nanometers to several microns. Pretreatment in NaOH/urea had no effect on the chemistry and crystalline structure of cellulose but decreased the degree of crystallinity. In a further study, cellulose nanocrystals (CNCs) were prepared from bleached OPT pulp by a Ni(II)-based hydrolysis process [19]. The resulting nanocrystals showed a cellulose content of almost 94%, an average diameter of 52 ± 3 nm, and a length of 440 ± 45 nm. As compared to CNCs from other sources like banana peel or coconut husk prepared by the same procedure, OPT-nanocrystals were characterized by a greater diameter and somewhat lower thermal stability as revealed by thermogravimetry. Okahisa et al. [21] compared the properties of CNFs prepared from different parts of the oil palm tree, i.e., trunk (OPT), empty fruit bunch (EFB), mesocarp, and palm kernel shell (PKS). While the cellulose content was roughly the same for OPT, mesocarp, and EFB, OPT showed the highest hemicellulose and lowest lignin content of all plant parts. Moreover, the individual starting materials differed in cellulose crystallinity with the highest value found in the trunk. The authors applied a bleaching process and mechanical fibrillation in a disc grinder to obtain CNFs which have then been processed into thin sheets for mechanical characterization. Normalized to a density of 1 g/cm^3, sheets prepared from OPT displayed a tensile strength of 157 ± 9 MPa and Young's modulus of 5.0 ± 0.3 GPa which again were the highest values among the various starting materials. In a more recent study by the same research group, CNFs were prepared from bleached OPT and used for mechanical reinforcement of poly(vinyl alcohol) (PVA) films [22]. Aside from the successful reinforcement of PVA, an average fibril diameter of 40 nm, tensile strength of around 220 MPa, and Young's modulus of 18.1 GPa were reported for pure CNF-sheets. Abdul Razab et al. [23] removed the non-cellulosic constituents of OPT fibers by an alkaline pretreatment process and applied high-intensity ultrasonication to obtain CNFs. Depending on the microscopic technique used, the authors report an average fibril diameter of 11 ± 6 nm (from TEM images) and 23 ± 6 nm (from FE-SEM images). Besides high L/D-ratio CNFs, a considerable number of markedly shorter nanocrystals (CNCs) were found.

In all the studies mentioned above, OPT has been chemically purified to yield bleached fibers which have then been used for the preparation of NC. However, certain amounts of residual hemicelluloses and lignin have been shown to positively affect both the fibrillation process and fibril properties. Depending on their type

Zaini *et al. Journal of Wood Science*   (2024) 70:19

Page 3 of 16

and content, residual non-cellulosic cell wall polymers have been reported to facilitate fibrillation [24–27], increase fibril yield [26], affect suspension viscosity [28, 29] and accelerate dewatering [24, 30]. As proposed by Ferrer et al. and Jiang et al. [25, 27], the easier fibrillation may be attributed to a dual mechanism consisting of increased swelling caused by hemicelluloses and formation of mechanoradicals stabilized by residual lignin. As far as nanopaper properties are concerned, potential effects of non-cellulosic cell wall constituents include lower nanopaper porosity and air permeability [24, 25], increased UV-absorption [27], improved mechanical properties [25, 28, 31, 32], lower thermal stability [28], as well as increased hydrophobicity and/or lower water uptake [24, 28, 30, 31]. The use of cellulose nanofibers with a high content of residual lignin and/or hemicelluloses has also been reported as beneficial for the preparation of cellulose nanocomposites [33–35].

The present study investigates the effect of delignification and mechanical fibrillation degree of OPT on the properties of the resulting micro- and nanofibrils. For this purpose, OPT was first delignified to varying degrees (non-delignified, partially and fully delignified) and subjected to mechanical fibrillation in two intensity levels (Masuko grinding with/without subsequent high-pressure homogenization). The resulting fibrils were characterized in terms of size and morphology, chemical composition, thermal stability, as well as rheological and sedimentation behavior in suspension.

Experimental
Materials
A 30-year-old OPT (*Elaeis guineensis* Jacq.) was harvested in Bogor (Indonesia) and further disintegrated at IPB University (Forest Products Department, Faculty of Forestry and Environment). First, the outer part of the trunk (roughly one-third) was removed and the remaining inner part was cut into chips which were subsequently dried to a moisture content of 10–12%. The chips were ground with a Wiley mill using a 60-mesh screen. The powder was oven-dried at 60 °C to 5% moisture content and shipped to BOKU University (Institute of Wood Technology and Renewable Materials, Tulln, Austria). For investigating the effect of delignification and fibrillation degree, 6 different treatments were applied to the ground raw material (OPT) resulting in 6 samples (OPT, M-OPT, MH-OPT, A-M-OPT, A-MH-OPT, B-H-OPT). In the sample name, *A* and *B* indicate the chemical pretreatment (*A* = Alkali-pretreated, *B* = bleached), while *M* and *H* denote the mechanical treatment (*M* = Masuko grinder, *H* = high-pressure homogenizer). For instance, A-MH-OPT denotes a sample that has been alkali-pretreated, Masuko-treated, and homogenized.

Delignification and fibrillation of OPT
Alkali-pretreatment was performed by soaking the OPT powder in a 1 wt% NaOH solution at room temperature for 48 h after which the supernatant (NaOH solution) was removed. OPT particles were equally transferred to four 500-mL centrifuge bottles, filled up with deionized (DI) water, and centrifuged for 5 min at 10,700 x *g*. Again, the supernatant was removed, new water was added and a pH of 7 was adjusted with 3 M HCl. Full delignification of OPT was achieved by an alkaline pulping process followed by hydrogen peroxide bleaching as described elsewhere [36]. Initially, OPT was delignified in a boiling solution of NaOH (2.5 mol/L) and Na_2SO_3 (0.4 mol/L) at a solid/liquid ratio of 1:6 for 8 h under continuous stirring. Thereafter, the material was bleached in 2.5 M H_2O_2 at 60 °C, again using a solid/liquid ratio of 1:6. In total, 3 bleaching steps with a duration of 3 h each were performed. Approximately 3 g of bleached fibers were rinsed 3 times with 500 mL DI water each. Samples without chemical pretreatment (M-OPT, MH-OPT) were further disintegrated by milling in a Retsch ZM 200 ultracentrifugal mill (Retsch GmbH, Haan, Germany) and the resulting powder was sieved using a 0.2-mm screen. The powder was soaked in DI water at 1% consistency overnight after which the swelled fibers were pre-crushed in a kitchen blender for 1 min. The suspensions were then processed by 10 passes through a Masuko MKCA6-2J disc grinder (Masuko Sangyo Co. Ltd., Kawaguchi, Japan). A nominal gap size of 0.1, 0.05, 0, − 0.05, and − 0.1 mm between the grinding discs was set and 2 passes were performed for each setting. If applicable, the last disintegration step was performed by 10 passes (2 passes each at 300 and 500 bar followed by 6 passes at 700 bar) in an APV-1000 high-pressure homogenizer (APV Manufacturing Poland Sp. Z o.o., Bydgoszcz, Poland).

Characterization
Microscopy
In order to study the effects of the treatments on fibril morphology, scanning electron microscopy (SEM) images were acquired on a Hitachi TM3030 tabletop microscope (Hitachi High-Technologies Corporation, Tokyo, Japan). For the preparation of SEM samples, one drop of the respective fibril suspension was placed on a mica disc and left to dry at room temperature overnight. For the OPT sample, the dry powder was directly placed on the mica disc. All samples were sputter-coated with 5 nm of platinum. For SEM imaging, an acceleration voltage of 20 kV was used. To obtain high-resolution topography images of CNFs, a Dimension Icon atomic force microscope (AFM) equipped with a ScanAsyst

Zaini *et al. Journal of Wood Science*   (2024) 70:19

Page 4 of 16

Air cantilever (Bruker, USA) was used. The samples were prepared by placing a drop of diluted nanofiber suspension (0.001 wt%) onto a freshly cleaved mica disc and subsequent drying at ambient conditions. The equivalent radius of the silicon tip was 2 nm. Data evaluation was carried out with the software Gwyddion 2.60. For each sample, the average fibril diameter was calculated as the geometric mean of the height of 15 individual fibrils.

Particle size distribution

The size of fibril agglomerates was studied using a Qicpic™ particle size analyzer (Sympatec GmbH, Clausthal-Zellerfeld, Germany) equipped with a Lixell module for analysis of particles in suspension. All measurements were performed with a 1-mm cuvette which, along with the M5 module used, is capable of detecting particles in the size range of 1.8–3755 μm. All suspensions were first adjusted to a concentration of 0.1 g/L with DI water. During the measurement, the suspension was stirred at 250 rpm and fed into the device by means of a peristaltic pump. Images were continuously acquired for a duration of 10 s at a frame rate of 85 Hz resulting in a total number of 10^5 to 10^6 particles analyzed. For each sample, 3 measurements were performed and the circle equivalent diameter (CED) was determined as a measure for particle size.

Fourier transform infrared spectroscopy (FT-IR)

For FT-IR spectroscopy, thin films were prepared by casting the fibril suspension into a petri dish and evaporation of water at room temperature over 3 days. The dried films with a thickness of around 200–300 μm were then cut into smaller pieces. Five layers of the same film were stacked on top of each other and measured in a Frontier FT-IR spectrophotometer (PerkinElmer, Waltham, MA, USA) using attenuated total reflection (ATR). For the OPT sample, the dry powder was used directly. For each sample, 3 measurements were performed in the region of 4000–600 cm^{-1}. All spectra were post-processed by a linear baseline correction and normalized using the peak maximum at around 1030 cm^{-1}.

Hemicellulose and lignin content

Acid methanolysis according to [37] and subsequent gas chromatography was used to determine the hemicellulose content of OPT fibers. For each sample, 3 measurements were performed. In brief, 2 mL of a 2 M solution of HCl in anhydrous methanol were added to approximately 10 mg of the sample and stored in an oven at 100 °C for 4 h. After cooling the sample to room temperature, about 100 μL of pyridine were added for neutralization.

Furthermore, 4 mL of methanol containing 0.1 mg/mL of sorbitol as an internal standard was added. A pear-shaped flask was filled with 1 mL of the clear sample solution to prevent the introduction of fibers during the subsequent silylation process. The material was dried at 40 °C for 20 min in a vacuum desiccator and the residue was dissolved by adding 70–100 μL of pyridine. For silylation, 150 μL of hexamethyldisilazane (HMDS) and 80 μL of trimethylchlorosilane (TMCS) were added to the sample which was then stored at room temperature overnight before GC–MS analysis.

For GC–MS, an Agilent 7890B GC system (Agilent Technologies, Mississauga, ON, Canada) equipped with a flame ionization detector (FID) was used. For all samples, the injection volume and split ratio were 1 μL and 10:1, respectively. Analyses were performed on an HP-1 methyl siloxane column (Agilent 19091Z-413, 30 m × 320 μm × 0.25 μm) with hydrogen as a carrier gas (2 mL/min). The oven temperature was maintained at 140 °C for 1 min and raised to 210 °C with a rate of 4 °C/min. Subsequently, rapid heating (30 °C/min) to a final temperature of 260 °C was performed which was maintained for 5 min. The FID was kept at 320 °C, with a hydrogen flow rate of 30 ml/min. For each sugar monomer present in the hemicelluloses, a calibration was carried out to calculate the amount from the peak area. Therefore, methanolysis, silylation, and GC–MS analysis on two separate samples containing each 0.1 mg of analytical grade arabinose, xylose, galactose, glucose, mannose, rhamnose, glucuronic acid, and galacturonic acid were performed. A calibration factor was calculated by relating the peak areas of the various sugar units to the peak area of the internal standard sorbitol.

The acid-insoluble lignin content of chemically treated samples was determined following the TAPPI T222 om-02 standard [38]. In short, the samples were first Soxhlet-extracted using a 2:1 (v/v) mixture of toluene/ethanol for a total of 4 h. A sample amount equivalent to ~ 1 g (OPT, A-MH-OPT) or 2 g (B-H-OPT) of dry weight, respectively, was analytically weighed into a 50-mL beaker. The beaker was placed in an ice bath and 15 mL of 72 wt% sulfuric acid was gradually added to the sample. The mixture was stirred with a glass rod, covered with a watch glass and left to stand for 2 h with occasional stirring. The hydrolyzed sample was then quantitatively transferred into a 1000-mL Erlenmeyer flask and filled up to a total volume of 575 mL with deionized water. The flask was covered with a watch glass and the sample was boiled in the diluted sulfuric acid for 4 h under continuous stirring (150 min^{-1}) and occasional addition of water to maintain the initial volume. After cooking, the suspension was left to stand at room temperature over night for full precipitation and vacuum-filtrated using a

Zaini *et al. Journal of Wood Science*   (2024) 70:19

Page 5 of 16

35-mL porcelain filter crucible (8 μm). The filter cake was rinsed with deionized water until a pH of 7 was achieved. The filled crucible was oven-dried at 103 °C for 4 h and the dry weight of the remaining acid-insoluble lignin was determined. Each sample was analyzed in duplicates. The Klason lignin content was determined according to Eq. (1):

$$\%\text{Lignin} = \frac{A}{W} \times 100, \tag{1}$$

where A = dry weight of acid-insoluble lignin (g) and W = initial dry weight of the sample (g).

Thermogravimetric analysis (TGA)

TGA experiments were carried out using a Netzsch TG 209 F1 Iris instrument (Netzsch-Gerätebau GmbH, Selb, Germany). Thermograms were acquired in the temperature range of 20–600 °C at a heating rate of 10 K/min, with nitrogen as purge gas at a flow rate of 250 mL/min. TGA samples were prepared from the same films as the FT-IR samples. TGA analysis was performed using approximately 10 mg of sample in an 85 μL aluminum oxide crucible with pierced lid. For each sample, measurements were carried out in duplicate. Thermograms were further processed by the software Netzsch Proteus analysis.

Rheology

For rheological characterization, an Anton Paar MCR 302 rheometer (Anton Paar GmbH, Graz, Austria) equipped with a cone/plate measuring system was used. Cone diameter, angle and truncation were 50 mm, 1°, and 0.1 mm, respectively. For each measurement, 2.4 mL of the 1 wt% suspension was placed on the plate with a syringe. All measurements were performed at 20 °C with a gap size of 1 mm. For assessing the shear rate and time-dependency of the viscosity, measurements were performed at both linearly increasing shear rate ($1-100$ s^{-1}) and a constant shear rate of 10 s^{-1} for 120 s. For each sample, 3 measurements were performed.

Zeta potential

The zeta potential of fibrillated and raw OPT in an aqueous medium was measured using an electrokinetic analyzer (SurPass, Anton Paar, Graz, Austria). Experiments were performed in a cylindrical cell with around 5 mL of a 2% (w/v) suspension. 0.001 M KCl solution was used as the medium for zeta potential measurement while 0.05 M KOH was added before each measurement in order to adjust the pH to 7. The zeta potential was determined at a temperature of 20 °C.

Sedimentation

For each sample group, the 1 wt% suspension was diluted to 0.25 wt% and transferred to 10-mL glass tubes. All tubes were initially shaken, put into a rack side by side, and left to stand at room temperature for 24 h. In order to assess fibril sedimentation, images were taken after 0 min, 1 min, 5 min, 40 min, 9.5 h, and 24 h.

Results and discussion
Microscopic characterization

The microstructure of the differently treated OPT samples can be assessed from low-magnification SEM images (Fig. 1). The ground starting material contains mostly vascular bundles (V) and parenchyma tissue (P) (Fig. 1a).
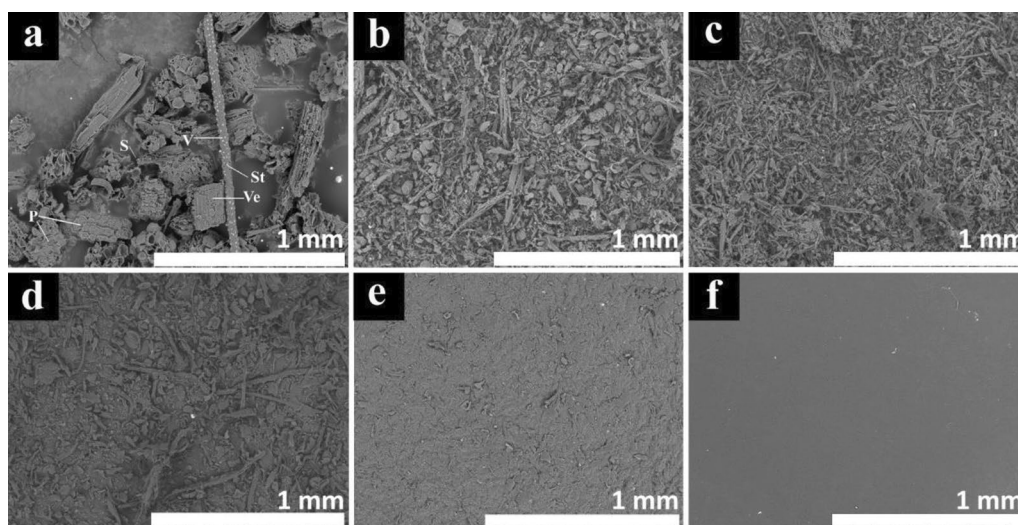

Fig. 1 SEM-images of **a** OPT, **b** M-OPT, **c** MH-OPT, **d** A-M-OPT, **e** A-MH-OPT, **f** B-H-OPT

Zaini *et al. Journal of Wood Science*   (2024) 70:19

Page 6 of 16

Vascular bundles consist of fibers, vessels (Ve) or metaxylem, protoxylem, protophloem or sieve tubes, axial parenchyma, stegmata (St), and companion cells. In addition, individual starch granules (S) are obvious in Fig. 1a. During ultracentrifugal milling, the parenchymatous tissue has been broken down and the length of vascular bundles was reduced. As to be expected, mechanical fibrillation of OPT not subjected to any chemical pretreatment leads to a size reduction of the individual cells which was more pronounced when Masuko grinding was combined with high-pressure homogenization (Fig. 1c) as compared to grinding only (Fig. 1b). Due to the relatively loose structure of the OPT tissue, mechanical fibrillation seems to primarily cause a separation into individual cells (parenchyma granules, vessels, fiber bundles) which can be distinguished in Fig. 1b. Alkali-pretreatment of OPT leads to a substantial weakening of the material structure by swelling and leaching of structural cell wall constituents. While individual cells and larger cell fragments are still apparent after grinding (Fig. 1d), those larger particles have been completely fibrillated during subsequent homogenization (Fig. 1e). In both cases, a continuous phase is evident, indicating the presence of a fine fibril fraction which, due to the low magnification used, appears quite homogeneous. The formation of a continuous layer of cellulose microfibrils can also be observed in paper if added in sufficient quantities [39]. Since lignin and hemicelluloses have been largely removed in the fully delignified OPT sample, the remaining network of interconnected cellulose fibrils appears as a homogenous,

untextured phase in low-magnification SEM images (Fig. 1f).

In order to visualize the fine structure of the different OPT samples and reveal differences in fibril size and morphology, AFM imaging was performed (Fig. 2). The non-delignified samples M-OPT and MH-OPT show a compact structure with cellulose fibrils still being interconnected by an amorphous phase of hemicelluloses and lignin (Fig. 2a, b). The latter was at least partially removed by chemical pretreatment which, after mechanical fibrillation, results in the liberation of individual CNFs (Fig. 2c–e). It can be seen that additional fibrillation in a high-pressure homogenizer significantly decreases the fibril diameter of alkali-treated OPT from 66 ± 14 nm for A-M-OPT to 16 ± 3 nm for A-MH-OPT. It appears that the energy input of Masuko grinding alone is not sufficient to fully individualize fibril bundles. This suggests that residual lignin in A-M-OPT did not act as a facilitator for mechanical defibrillation as suggested by Ferrer et al. [25]. However, residual lignin might represent a physical barrier that slows down the fibrillation process by a defibrillation delay mechanism [40]. In addition, residual lignin might serve as a binding agent to the surface of nanofibers, resulting in complex structures with low entanglement ability thus resisting mechanical fibrillation [41]. The bright dots appearing in Fig. 2d might represent nano-scale lignin particles attached to the cellulose nanofibers. The size and shape of these lignin nanoparticles complies well with the findings of a previous study [42]. It is worth noting that the nanostructure of
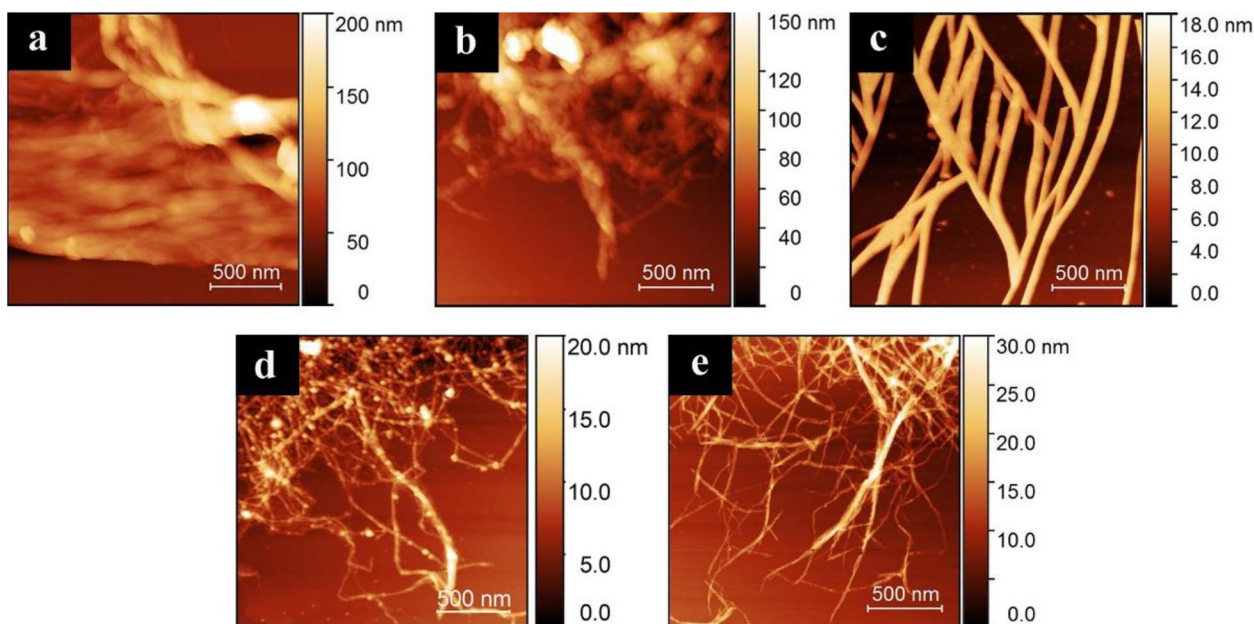

Fig. 2 AFM-images of **a** M-OPT, **b** MH-OPT, **c** A-M-OPT, **d** A-MH-OPT, **e** B-H-OPT

Zaini *et al. Journal of Wood Science*   (2024) 70:19

Page 7 of 16

A-MH-OPT is very similar to fully delignified B-H-OPT, although far less severe chemical treatment was used. This is also reflected by a similar fibril diameter, which is even a bit lower for A-MH-OPT (16±3 nm) than for B-H-OPT (21±4 nm). In general, the fibril diameters found in the present study correspond well to previous findings. For instance, a diameter range of 10–100 nm was reported for CNFs prepared by high-pressure homogenization of bleached OPT fibers [20]. Depending on the microscopy technique used, Abdul Razab et al. [23] determined values of 11±6 nm by transmission electron microscopy (TEM) and 23±6 nm by field emission scanning electron microscopy (FE-SEM), respectively, for OPT nanofibrils prepared by high-intensity ultrasonication of bleached OPT fibers.

Particle size distribution

While individual nanofibrils were characterized by AFM, a particle size analyzer was used to study the presence of larger fibril agglomerates on the micro- and macroscale. Figure 3 depicts the distribution of CED values for all OPT samples. Not surprisingly, the non-fibrillated OPT sample shows a distinct peak at a CED between 100 and 1000 μm, indicating the presence of a high portion of large particles. Differences between the fibrillated OPT samples are particularly evident from the cumulative frequency distribution. It can be seen that B-H-OPT generally showed the smallest CED

values closely followed by A-MH-OPT which displays a very similar particle size distribution. As far as the fibrillation technique is concerned, all high-pressure homogenized samples clearly showed less coarse particles and more fines than samples fibrillated by Masuko grinding only. Thus, the fibrillation technique is essentially affecting particle size distribution. For homogenized samples, additional alkali-pretreatment further shifted the distribution towards smaller CED values (MH-OPT vs. A-MH-OPT), while this could not be observed for Masuko-treated samples (M-OPT vs. A-M-OPT). The removal of hemicelluloses and lignin generates nanospaces between the cellulose fibrils in the cell wall, which improve mechanical defibrillation ultimately resulting in lower CED values [43]. On the other hand, hemicelluloses play a role as physical barrier preventing close contact and further aggregation of cellulose fibrils by impeding the formation of interfibrillar hydrogen bonds [44]. This mechanism facilitates mechanical fibrillation and could be responsible for the smaller CED values of M-OPT. It needs to be stressed that the combination of alkali-pretreatment, Masuko grinding and high-pressure homogenization of OPT revealed a particle size distribution very similar to that of CNFs prepared from fully delignified OPT particles.
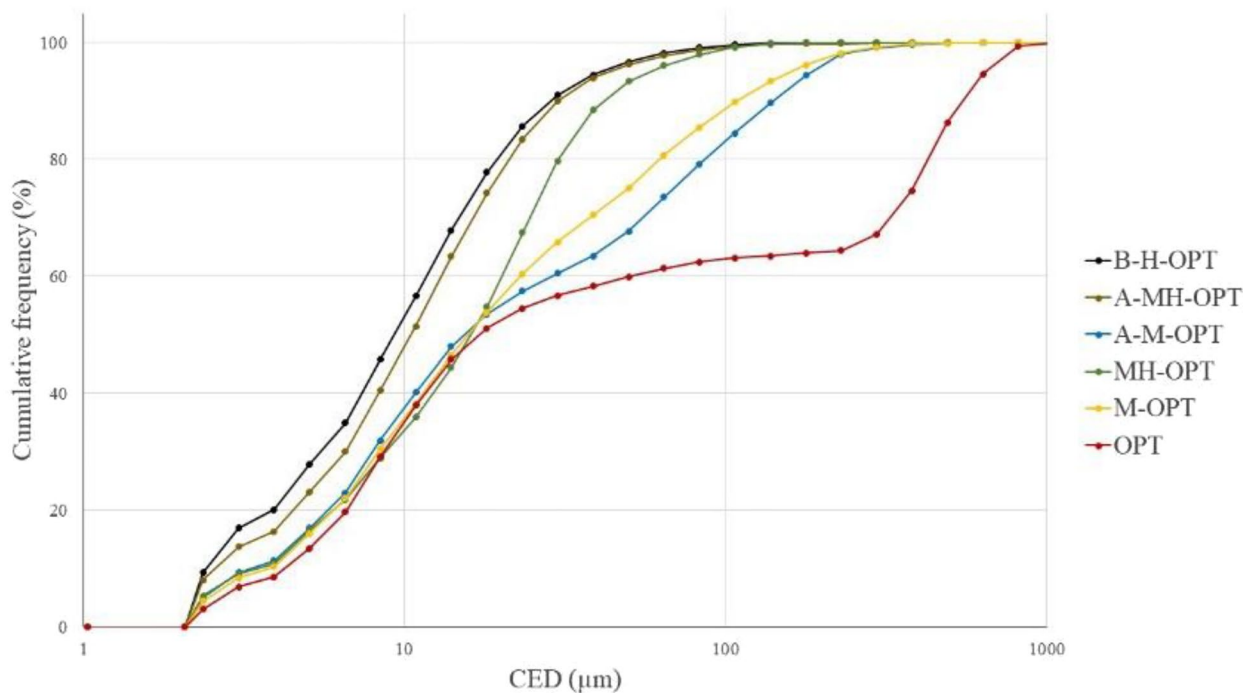

Fig. 3 Cumulative frequency distribution of area-weighted circle equivalent diameter (CED) of OPT-fibril agglomerates

Zaini *et al. Journal of Wood Science* (2024) 70:19

Page 8 of 16

FT-IR analysis

FT-IR spectroscopy was used for observing changes in the chemical composition of samples in response to various treatments. The FT-IR spectra of all untreated and treated samples are shown in Fig. 4. As one would expect, mechanical treatment did not affect the chemical composition of OPT indicated by very similar FT-IR spectra for OPT, M-OPT, and MH-OPT. However, partial delignification by alkali-pretreatment already had a notable effect and after complete delignification by bleaching, samples rather showed an FT-IR spectrum typical to pure cellulose. In the OPT, M-OPT, and MH-OPT spectra, three notable bands at around 1735 cm^{-1}, 1371 cm^{-1}, and 1235 cm^{-1} are evident but widely disappear in the spectra of chemically treated samples. The bands at 1735 cm^{-1} and 1235 cm^{-1} can be attributed to C=O and C–O stretching in ester groups of xylans

(hemicelluloses), whereas the peak at 1371 cm^{-1} arises from C–H deformation in cellulose and hemicelluloses [17]. The three bands mentioned above are primarily attributed to the presence of acetyl groups, as they were found to increase with increasing acetyl content in acetylated wood [45, 46]. The disappearance of the bands at 1735 cm^{-1}, 1371 cm^{-1} and 1235 cm^{-1} for alkali-treated and bleached samples thus indicates deacetylation of hemicelluloses under the chosen conditions. Besides structural changes like cleavage of acetyl groups, hemicelluloses did apparently not undergo significant hydrolysis and largely remained in the material as the concentration of xylose and 4-*O*-methylglucuronic acid (4-OMeGlcUA) did not change markedly upon alkali-pretreatment thus indicating the presence of xylan in A-MH-OPT (Table 1). This is in line with the findings of Laine et al. [47] who reported that under mild
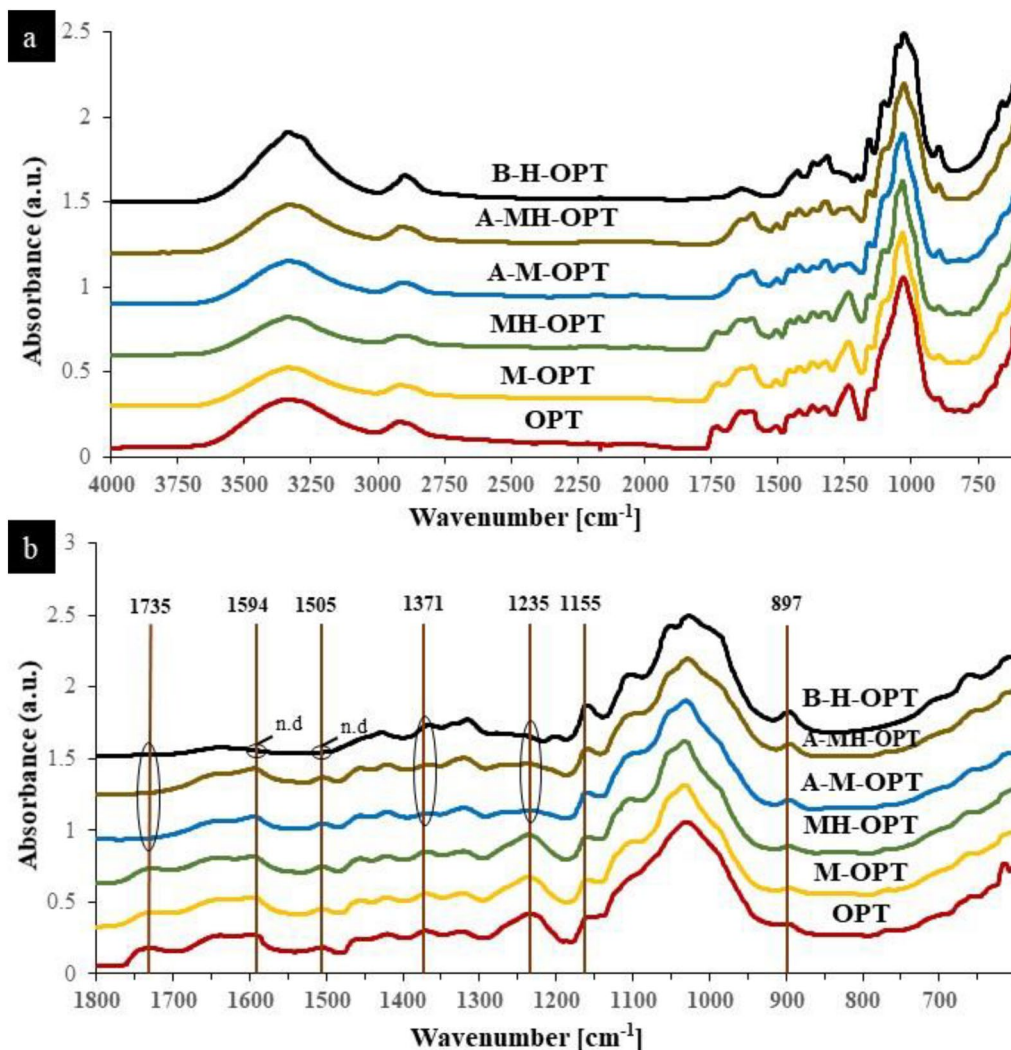

Fig. 4 FT-IR spectra ranging from 4000–600 cm^{-1} (**a**) and 1800–600 cm^{-1} (**b**) of OPT-fibrils with different delignification and fibrillation treatments

Zaini *et al. Journal of Wood Science*   (2024) 70:19

Page 9 of 16

Table 1 Hemicellulose content (%), sugar composition (in µg/mg dry matter) and Klason lignin content (%) of raw and chemically treated oil palm trunk

	OPT	A-MH-OPT	B-H-OPT
Hemicellulose	31.5	29.5	17.8
Arabinose	16.2	14.6	1.1
Rhamnose	3.6	3.3	0.2
Fucose	1.6	1.8	–
Xylose	176.7	189.3	38.5
GalUA	13.5	14.0	–
4-OMeGlcUA	32.2	29.7	1.3
Mannose	9.7	4.2	0.5
Galactose	8.4	6.4	0.5
Glucose	50.5	30.9	135.4
GlcUA	1.9	1.2	0.5
myo-Inositol	0.3	–	–
Lignin	24.3	20.1	1.4

alkaline pre-treatment conditions, hemicelluloses remain mostly intact but experience different chemical changes like removal of acetyl and uronic acid groups as well as saponification of ester bonds that link hemicellulose to other lignocellulosic components. The bands at around 1594 and 1505 cm^{-1} are assigned to aromatic skeletal vibration in lignin [17] and may thus serve as an indicator for assessing the extent of lignin removal. With the exception of B-H-OPT, the two lignin bands occur to almost the same extent in all samples, suggesting that only the bleaching treatment has effectively removed lignin, while it largely remained after alkali-treatment. The higher relative carbohydrate content of B-H-OPT is also obvious from the more pronounced peaks at around 897 and 1155 cm^{-1}, which correspond to C–H deformation in cellulose and C–O–C vibration in cellulose and hemicelluloses [17], respectively.

Chemical composition

The hemicellulose and lignin content of OPT, A-MH-OPT and B-H-OPT were determined according to [37] and [38]. The hemicellulose and lignin contents as well as the composition of hemicelluloses are shown in Table 1. The hemicellulose content was only marginally decreased by the alkali-treatment while the bleaching treatment removed almost half of the hemicelluloses present in the raw material. For OPT and A-MH-OPT, the hydrolysis of hemicelluloses resulted in a high xylose concentration, indicating that xylan is the most abundant hemicellulose in these samples. However, a significantly lower xylose concentration was found for B-H-OPT, suggesting that most of the xylan was removed during the bleaching treatment. The markedly higher glucose concentration might arise from partial hydrolysis of cellulose during methanolysis rather than from hemicelluloses. As for the lignin content, the raw material OPT shows a value of 24.3% which corresponds well to the findings of previous studies [12, 15, 48]. Similar to hemicelluloses, the lignin content decreased only moderately after mild alkali-pretreatment. This is in line with the findings of Wardani et al. [49], who reported no significant reduction in the lignin content of OPT after treatment with 5% NaOH at elevated temperature. At low alkali concentration (< 4%) and temperature (< 100 °C), alkali-pretreatment does typically not result in notable cellulose degradation or change of crystalline properties [50–52]. Even if the mild alkali-pretreatment applied herein did not significantly reduce the hemicellulose and lignin content, a substantial swelling effect can be achieved which clearly facilitates subsequent mechanical fibrillation. This is also reflected by the markedly lower fibril diameters observed for alkali-treated samples (A-M-OPT and A-MH-OPT) as opposed to their untreated counterparts (M-OPT and MH-OPT) in Table 2. Consequently, alkali-treatment as applied in this study, results in small fibrils

Table 2 Average diameter, particle size distribution, thermogravimetric, and surface charge properties of OPT-fibrils

	Avg. diameter by AFM analysis (nm)	Avg. CED by particle size analyser (µm)	Onset T (°C)	Peak T (°C)	Mass change (%)	Residual mass (%)	Zeta potential (mV) at pH 7
OPT	–	205 ± 22	253 ± 22	287 ± 4	28 ± 0.6	22 ± 0.8	− 15 ± 0.8
				348 ± 4	40 ± 3.9		
M–OPT	141 ± 51	46 ± 1.1	283 ± 16	300 ± 0.3	36 ± 0.7	22 ± 0.5	− 10 ± 1.2
				348 ± 1	48 ± 0.4		
MH–OPT	39 ± 17	24 ± 0.6	277 ± 7	301 ± 2	25 ± 0.6	23 ± 0.4	− 12 ± 0.7
				342 ± 2	46 ± 2		
A–M–OPT	66 ± 14	55 ± 0.8	279 ± 6	328 ± 1	68 ± 0.9	26 ± 1.1	− 6 ± 0.3
A–MH–OPT	16 ± 3	18 ± 0.5	278 ± 1	325 ± 5	62 ± 1.2	30 ± 1.6	− 7 ± 2.0
B–H–OPT	21 ± 4	16 ± 0.4	314 ± 1	343 ± 1	79 ± 0.3	15 ± 0.4	− 14 ± 1.5

Zaini *et al. Journal of Wood Science*   (2024) 70:19

Page 10 of 16

with a chemical composition similar to that of the raw material, i.e., with high hemicellulose and lignin content. As already mentioned in the introduction, the presence of these non-cellulosic cell wall constituents in cellulose nanofibers can be beneficial in composite applications. For instance, they have been shown to improve fiber dispersion in non-polar matrix polymers like polylactic acid [34, 53] or polycaprolactone [54]. Contrary to alkali-pretreatment, the applied bleaching process removed lignin very effectively, indicated by a residual lignin content of only 1.4% for B-H-OPT. This finding is in perfect agreement with the FT-IR results, where the disappearance of the lignin-associated bands at 1594 and 1505 cm^{-1} also suggested the virtual absence of lignin in this sample.

Thermal properties

The TGA curves of all samples are shown in Fig. 5 and the specific values are provided in Table 2. With all samples, water evaporation caused an early weight loss at temperatures around 100 °C. Thermal degradation of lignocellulosic materials usually starts with hemicellulose decomposition, followed by lignin pyrolysis, cellulose depolymerization, active flaming combustion, and finally char oxidation [55]. Hemicelluloses are the structural constituent with the lowest thermal stability, initiating to decompose at 220–315 °C, while lignin degrades in a wide temperature range of 100–900 °C [56], thus overlapping the degradation of polysaccharides. Sample

decomposition already started at an onset-temperature of about 250 °C for OPT and increased to 280 °C for alkali-treated and 315 °C for bleached OPT samples (Fig. 5, Table 2). Largely reflecting the specimens' hemicellulose and lignin content, the initial DTG decomposition peak was most pronounced for OPT, somewhat less obvious for M-OPT and MH-OPT, diminishing to a weak shoulder for alkali-treated samples which finally disappeared almost entirely for fully delignified B-H-OPT. Since it primarily contains purified cellulose, B-H-OPT only displayed one quite narrow decomposition peak at around 345 °C associated with cellulose degradation which has been reported to occur between 315 and 400 °C [57]. Interestingly, the decomposition peak of cellulose is shifted to a lower temperature of around 325 °C for A-M-OPT and A-MH-OPT. This might be due to the coincidence of cellulose and residual hemicellulose/lignin degradation which was particularly obvious for alkali-treated samples. The initial pyrolysis temperature of lignin is known to be lower than for cellulose [58, 59] which could explain the left-shift of the peak temperature. At temperatures higher than 500 °C, the curves of all samples nearly straighten out since only thermally inert carbon and inorganic compounds remain as a residue [6]. Considering the residual mass of the individual samples (Table 2), it is striking that the alkali-treated samples display a higher value than the raw OPT, which can be primarily explained by insufficient removal of NaOH
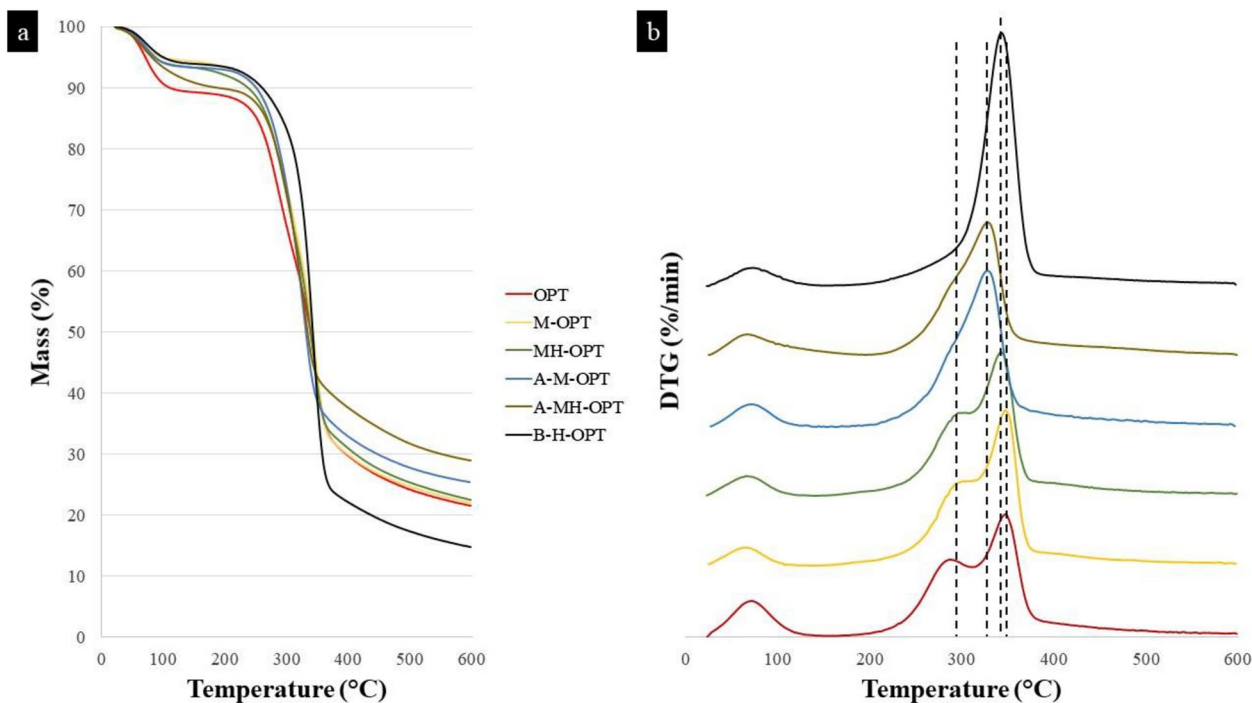

Fig. 5 TG (**a**) and DTG (**b**) curves of OPT-fibrils with different delignification and fibrillation treatments

after the treatment and subsequent salt formation during neutralization with hydrochloric acid. On the other hand, B-H-OPT shows a residual mass around one-third lower than for the starting material OPT. This might be attributed to the extensive removal of lignin whose carbon content (63–66%) is significantly higher than that of cellulose (around 44%) [60]. Moreover, a higher portion of inorganic compounds might have been removed during the more severe pulping and bleaching procedure applied for this sample. OPT ash is known to consist of about 46% silica [61] whose solubility strongly increases at elevated pH and temperature [62] as applied in the preparation of B-H-OPT.

Rheological properties

Rheological properties are affected by the shape of the fibrillated fibers, surface characteristics, and production method [63]. The viscosity of fibril suspensions was measured as a supplementary indicator of fibrillation in conjunction with changes in fibril size and morphology as observed by microscopy techniques. The viscosity of OPT-fibril suspensions is depicted in Fig. 6. All samples demonstrate shear-thinning behavior (Fig. 6a), as can be expected for suspensions containing fibrils that are likely to arrange themselves and partially disentangle due to flow, resulting in a viscosity reduction with increasing shear rate. In terms of absolute values, B-H-OPT exhibited the highest viscosity, followed by A-MH-OPT,

A-M-OPT, MH-OPT, and M-OPT. Same as with particle size analysis, A-MH-OPT was found to behave very similarly to fully delignified OPT-CNF (B-H-OPT) although the absolute viscosity values were somewhat lower. Alkali-pretreatment seems to generally increase viscosity, while the samples lacking any chemical pretreatment were characterized by a very low viscosity. This is mainly attributed to the pronounced swelling effect of NaOH even at the low concentration used herein which facilitates mechanical fibrillation [31] and results in lower fibril diameters of alkali-pretreated samples (Table 2). The smaller fibril diameter leads to stronger interfibrillar interactions (entanglement, hydrogen bonding, etc.) which again increase the flow resistance and thus viscosity of the suspension [64]. The presence of a strong lignocellulose complex in non-delignified samples (MH-OPT and M-OPT) results in less individualized fibrils still covered by hemicelluloses and lignin for M-OPT and MH-OPT as observed in AFM images. The lower available fibril surface area strongly restricts fibril–fibril interactions and continuous network formation, ultimately reflected by a low sample viscosity. As obvious from Fig. 6b, all samples showed hardly any change of viscosity over time at a constant shear rate of 10 s^{-1}. It is also noteworthy, that the viscosity of the individual samples varied from around 50 mPa·s for M-OPT all the way to 13,500 mPa·s for B-H-OPT. The viscosity of
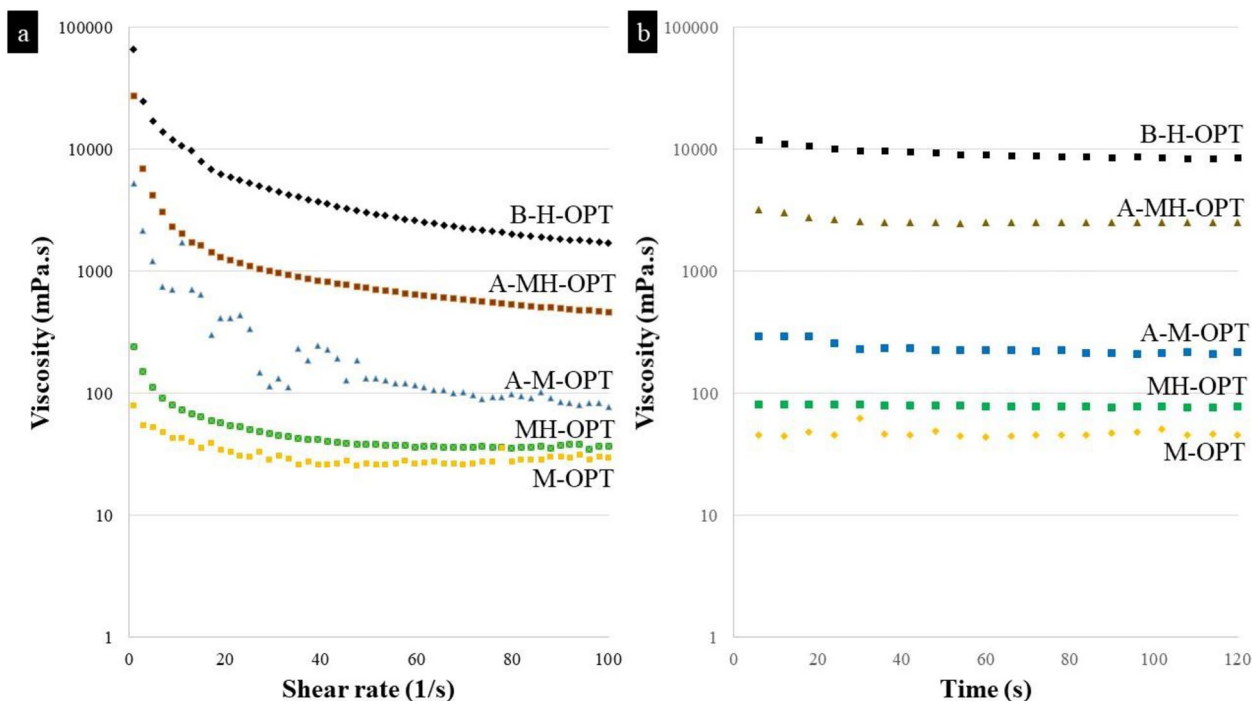

Fig. 6 Viscosity of 1 wt% OPT-fibril suspensions as a function of shear-rate (**a**) and time (**b**)

OPT-suspensions can therefore be varied in a wide range by choosing appropriate delignification and fibrillation conditions.

Surface charge of fibrils

The results of zeta potential analysis at pH 7 are shown in Table 2. OPT fibers display a negative surface charge of about − 15 mV in water suspension arising from surface group ionization (carboxyl, sulfo, catecholic, phenolic and hydroxyl groups), adsorption of suitable ions, or the structure of water at the solid–liquid interface [65]. The slightly higher zeta potential of M-OPT and MH-OPT as compared to the raw material OPT might be caused by the adsorption of metal ions from the Masuko grinder and/or homogenizer during processing [65]. Increasing the level of refining does not have a significant effect on the weak acid content or electrophoretic mobility [65]. Hence, subsequent high-pressure homogenization (MH-OPT) after Masuko treatment (M-OPT) has only a minor effect on zeta potential. The less negative zeta potential observed after alkali-treatment (A-M-OPT and A-MH-OPT) may be attributed to the removal of hydroxyl or carboxyl groups on the surface susceptible to dissociation at the OPT surface and/or aldehyde groups of hemicelluloses. Decreasing lignin content and removal or modification of hemicelluloses during alkali-treatment have been reported to decrease weak acid content and result in less negative electrophoretic mobility [65]. In addition, the presence of adsorbed alkali cations of NaOH-treated fibers may cause a shift towards less negative zeta potential values [66]. Even after bleaching, the OPT-nanofibrils show a rather low zeta potential due to the higher weak acid content induced by oxidation reflected by a more negative zeta potential [65]. However, considering the FT-IR spectra of B-H-OPT, the oxidation did not appear to proceed considerably, since the carbonyl content did not increase. This discrepancy could arise from differences in surface sensitivity which is extremely high for zeta potential but less pronounced for ATR-FT-IR. Hence, groups might be more easily detected during zeta potential measurements but harder to identify in FT-IR spectroscopy. The value of − 14 mV determined for B-H-OPT is also in good accordance with the findings of Cheng et al. [67] who reported a zeta potential of − 16.2 mV for CNFs from bleached softwood Kraft pulp.

Sedimentation

To empirically investigate the stability of fibril suspensions at a given concentration, a sedimentation test was carried out. As shown in Fig. 7, all samples displayed homogeneous particle distribution immediately after shaking (0 s), whereas, for OPT, M-OPT, MH-OPT, and A-M-OPT samples, noticeable sedimentation occurred already after 1 min indicating low sedimentation stability. Contrary to this, both B-H-OPT and A-MH-OPT show much higher stability with the first sedimentation phenomena appearing after 40 min and 9.5 h, respectively. According to Stokes' equation, sedimentation rate is a function of the squared particle radius, gravitational acceleration, the density difference between particle and fluid, and dynamic viscosity of the fluid. While the other factors might be assumed to be constant for all samples, great importance must be attached to differences in particle size. In general, the sedimentation results are in good agreement with average fibril diameters and CED values but correlate far less with zeta potential results (Table 2). The large particles present in OPT- and M-OPT samples cause fast sedimentation which is largely completed already after 1 min. The clearly smaller fibrils of A-M-OPT settle more slowly with full sedimentation occurring within 5 min. Corresponding to a further leap down in fibril diameter and CED, MH-OPT displays complete sedimentation after 40 min. Following this trend, A-MH-OPT and B-H-OPT, which showed the lowest fibril diameter and CED, were found most stable in the sedimentation test and behaved very similarly. Although for these two samples, the endpoint of the sedimentation was not reached, A-MH-OPT showed lower sedimentation than B-H-OPT after 40 min, 9.5 h, and 24 h, indicated by a lower height of the precipitate. At comparable average fibril diameter and CED, the zeta potential of A-MH-OPT was about half that of B-H-OPT. Since a higher zeta potential is usually accompanied by better dispersion stability due to higher inter-particulate repulsion forces (e.g., [68]), zeta potential may not serve as an explanatory variable in this regard. However, this may be explained by the generally low zeta values found in this study, since a zeta value of − 30 mV is usually considered optimal for good stabilization of a nano-dispersion [68]. Thus, the differences in zeta potential between the individual samples might simply be too small to perceptibly affect sedimentation.
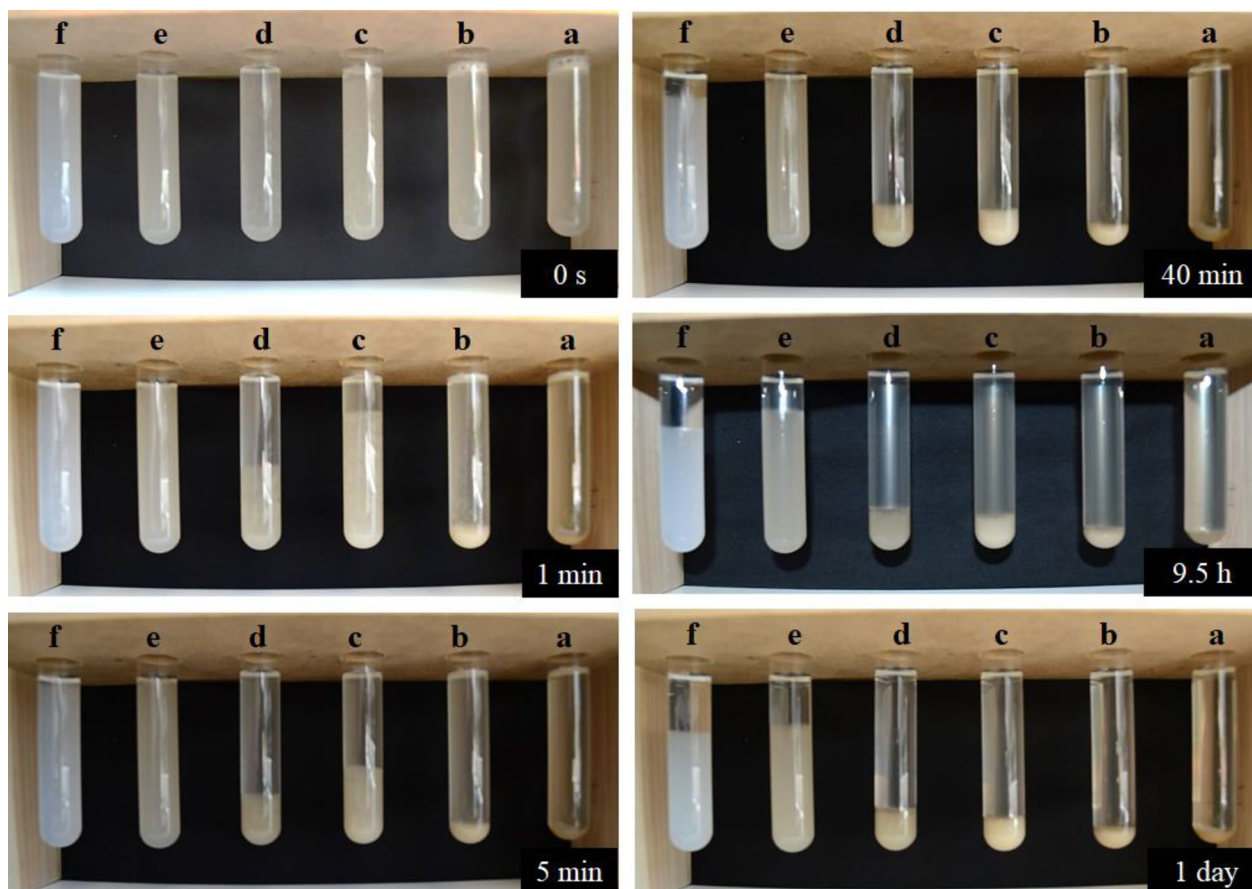
Zaini *et al. Journal of Wood Science*   (2024) 70:19

Page 13 of 16

Fig. 7 Time-dependent sedimentation of 1 wt% suspensions of **a** OPT, **b** M-OPT, **c** MH-OPT, **d** A-M-OPT, **e** A-MH-OPT, **f** B-H-OPT

Conclusions

Mechanical fibrillation of chemically non-pretreated OPT yields fibril agglomerates of high lignin and hemicellulose content which show low viscosity and poor suspension stability. Low-concentration alkali-pretreatment of OPT has been shown to have almost no effect on hemicellulose and lignin content, but results in considerably better individualization of nanofibrils reflected by a pronounced drop in average fibril diameter. Moreover, alkali-treated OPT samples showed higher viscosity and increased sedimentation stability as compared to their non-pretreated counterparts. Additional high-pressure homogenization after grinding strongly reduced the average fibril diameter and CED of both, non-pretreated and alkali-pretreated samples. Noteworthy, the combination of alkali-pretreatment and mechanical fibrillation by grinding and subsequent homogenization resulted in OPT fibrils which, in terms of fibril dimensions, presence of fibril agglomerates, viscosity and sedimentation rate, behaved similarly to fibrils from fully delignified OPT. Hence, this treatment represents an opportunity to directly prepare nanofibrils from unbleached OPT without the necessity for a chemically and energy-intensive delignification process. Notwithstanding the obvious differences in anatomy, this approach could also be successfully applied to hardwoods, since their chemical composition is similar to that of OPT.

Abbreviations

A-MH-OPT	Alkali Masuko Homogenized OPT
A-M-OPT	Alkali Masuko OPT
AFM	Atomic force microscope
ATR	Attenuated total reflection
B-H-OPT	Bleached homogenized OPT
CNCs	Cellulose nanocrystals
CNFs	Cellulose nanofibrils
CED	Circle equivalent diameter
DI	Deionized
EFB	Empty fruit bunch
FE-SEM	Field emission scanning electron microscope
FT-IR	Fourier transform infrared spectroscopy
MH-OPT	Masuko homogenized– OPT
M-OPT	Masuko OPT

NC	Nanocellulose
OPT	Oil palm trunk
PKS	Palm kernel shell
PVA	Poly(vinyl alcohol)
SEM	Scanning electron microscopy
TEM	Transmission electron microscope
TGA	Thermogravimetric analysis

Availability of data and materials
The datasets used and/or analyzed during the current study are available from the corresponding author on reasonable request.

Declarations

Ethics approval and consent to participate
Not applicable.

Consent for publication
Not applicable.

Competing interests
The authors have no competing interests as defined by Springer, or other interests that might be perceived to influence the results and/or discussion reported in this paper.

References
1. Hambali E, Rivai M (2017) The potential of palm oil waste biomass in Indonesia in 2020 and 2030. IOP Earth Environ Sci 65:012050
2. Ferrer A, Filpponen I, Rodriguez A, Laine J, Rojas OJ (2012) Valorization of residual Empty Palm Fruit Bunch Fibers (EPFBF) by microfluidization: production of nanofibrillated cellulose and EPFBF nanopaper. Bioresour Technol 125:249–255. https://doi.org/10.1016/j.biortech.2012.08.108
3. Yahya M, Lee H, Zain S, Abd Hamid S (2015) Chemical conversion of palm-based lignocellulosic biomass to nano-cellulose. Polym Res J 9(4):385
4. Bukhari NA, Jahim JM, Loh SK, Nasrin AB, Luthfi AAI (2019) Response surface optimisation of enzymatically hydrolysed and dilute acid pre-treated oil palm trunk bagasse for succinic acid production. BioResources 14(1):1679–1693
5. Bakar ES, Sahri MH, H'ng PS, (2008) Anatomical characteristics and utilization of oil palm wood. In: Nobuchi T, Sahri MH (eds) The formation of wood in tropical forest trees—a challenge from the perspective of functional wood anatomy. UPM Press, Finland, pp 161–178
6. Lamaming J, Hashim R, Leh CP, Sulaiman O, Sugimoto T, Nasir M (2015) Isolation and characterization of cellulose nanocrystals from parenchyma and vascular bundle of oil palm trunk (*Elaeis guineensis*). Carbohyd Polym 134:534–540
7. Lamaming J, Hashim R, Sulaiman O, Leh CP, Sugimoto T, Nordin NA (2015) Cellulose nanocrystals isolated from oil palm trunk. Carbohyd Polym 127:202–208
8. Mokhtar A, Hassan K, Aziz AA, Wahid M (2011) Plywood from oil palm trunks. J Oil Palm Res 23(3):1159–1165
9. Sulaiman O, Salim N, Nordin NA, Hashim R, Ibrahim M, Sato M (2012) The potential of oil palm trunk biomass as an alternative source for compressed wood. BioResources 7(2):2688–2706
10. Pennells J, Godwin ID, Amiralian N, Martin DJ (2020) Trends in the production of cellulose nanofibers from non-wood sources. Cellulose 27(2):575–593
11. Sjöström E, Westermark U (1999) Chemical composition of wood and pulps: basic constituents and their distribution. Analytical methods in wood chemistry, pulping, and papermaking. Springer, Berlin Heidelberg, pp 1–19
12. Abdul Khalil H, Siti Alwani M, Ridzuan R, Kamarudin H, Khairul A (2008) Chemical composition, morphological characteristics, and cell wall structure of Malaysian oil palm fibers. Polym-Plast Technol Eng 47(3):273–280
13. Tareen AK, Punsuvon V, Parakulsuksatid P (2020) Investigation of alkaline hydrogen peroxide pretreatment to enhance enzymatic hydrolysis and phenolic compounds of oil palm trunk. 3 Biotech 10(4):1–12
14. Sun R, Tomkinson J (2001) Fractional separation and physico-chemical analysis of lignins from the black liquor of oil palm trunk fibre pulping. Sep Purif Technol 24(3):529–539
15. Lamaming J, Hashim R, Sulaiman O, Sugimoto T, Sato M, Hiziroglu S (2014) Measurement of some properties of binderless particleboards made from young and old oil palm trunks. Measurement 47:813–819
16. Boon JG, Hashim R, Sulaiman O, Hiziroglu S, Sugimoto T, Sato M (2013) Influence of processing parameters on some properties of oil palm trunk binderless particleboard. Eur J Wood Wood Prod 71(5):583–589
17. Surip S, Bonnia NN, Anuar H, Hassan NA, Yusof NM (2012) Nanofibers from oil palm trunk (OPT): preparation & chemical analysis. In: 2012 IEEE Symposium on Business, Engineering and Industrial Applications, Bandung, Indonesia. pp. 809–812. https://doi.org/10.1109/ISBEIA.2012.6423003
18. Yahya M, Lee H, Abd Hamid SB (2016) Preparation of cellulose nanocrystals bio-polymer from agro-industrial wastes: separation and characterization. Polym Polym Compos 24:719–728. https://doi.org/10.1177/096739111602400907
19. Yahya M, Chen YW, Lee HV, Hassan WHW (2018) Reuse of selected lignocellulosic and processed biomasses as sustainable sources for the fabrication of nanocellulose via Ni(ii)-catalyzed hydrolysis approach: a comparative study. J Polym Environ 26(7):2825–2844. https://doi.org/10.1007/s10924-017-1167-2
20. Luo X, Wang X (2017) Preparation and characterization of nanocellulose fibers from NaOH/urea pretreatment of oil palm fibers. BioResources 12(3):5826–5837
21. Okahisa Y, Furukawa Y, Ishimoto K, Narita C, Intharapichai K, Ohara H (2018) Comparison of cellulose nanofiber properties produced from different parts of the oil palm tree. Carbohyd Polym 198:313–319
22. Okahisa Y, Matsuoka K, Yamada K, Wataoka I (2020) Comparison of polyvinyl alcohol films reinforced with cellulose nanofibers derived from oil palm by impregnating and casting methods. Carbohyd Polym 250:116907
23. Abdul Razab MKA, Mohd Ghani RS, Mohd Zin FA, Nik Yusoff NAA, Mohamed Noor AA (2021) Isolation and characterization of cellulose nanofibrils from banana pseudostem, oil palm trunk, and kenaf bast fibers using chemicals and high-intensity ultrasonication. J Nat Fibers 19:5537
24. Rojo E, Peresin MS, Sampson WW, Hoeger IC, Vartiainen J, Laine J, Rojas OJ (2015) Comprehensive elucidation of the effect of residual lignin on the physical, barrier, mechanical and surface properties of nanocellulose films. Green Chem 17(3):1853–1866

25. Ferrer A, Quintana E, Filpponen I, Solala I, Vidal T, Rodriguez A, Laine J, Rojas OJ (2012) Effect of residual lignin and heteropolysaccharides in nanofibrillar cellulose and nanopaper from wood fibers. Cellulose 19(6):2179–2193. https://doi.org/10.1007/s10570-012-9788-z

26. Jiang Y, Liu X, Yang Q, Song X, Qin C, Wang S, Li K (2018) Effects of residual lignin on mechanical defibrillation process of cellulosic fiber for producing lignocellulose nanofibrils. Cellulose 25(11):6479–6494. https://doi.org/10.1007/s10570-018-2042-6

27. Jiang Y, Liu X, Yang Q, Song X, Qin C, Wang S, Li K (2019) Effects of residual lignin on composition, structure and properties of mechanically defibrillated cellulose fibrils and films. Cellulose 26(3):1577–1593

28. Chen Y, Fan D, Han Y, Lyu S, Lu Y, Li G, Jiang F, Wang S (2018) Effect of high residual lignin on the properties of cellulose nanofibrils/films. Cellulose 25:6421–6431

29. Wen Y, Yuan Z, Liu X, Qu J, Yang S, Wang A, Wang C, Wei B, Xu J, Ni Y (2019) Preparation and characterization of lignin-containing cellulose nanofibril from poplar high-yield pulp via TEMPO-mediated oxidation and homogenization. ACS Sustain Chem Eng 7(6):6131–6139

30. Lê HQ, Dimic-Misic K, Maloney T, Johansson L-S, Sixta H (2018) Effect of lignin on the morphology and rheological properties of nanofibrillated cellulose produced from γ-valerolactone/water fractionation process. Cellulose 25(1):179–194

31. Nair SS, Yan N (2015) Effect of high residual lignin on the thermal stability of nanofibrils and its enhanced mechanical performance in aqueous environments. Cellulose 22(5):3137–3150

32. Santucci BS, Bras J, Belgacem MN, da Silva Curvelo AA, Pimenta MTB (2016) Evaluation of the effects of chemical composition and refining treatments on the properties of nanofibrillated cellulose films from sugarcane bagasse. Ind Crops Prod 91:238–248

33. Winter A, Mundigler N, Holzweber J, Veigel S, Müller U, Kovalcik A, Gindl-Altmutter W (2018) Residual wood polymers facilitate compounding of microfibrillated cellulose with poly (lactic acid) for 3D printer filaments. Philos Trans R Soc A Mathe Phys Eng Sci 376(2112):20170046

34. Winter A, Andorfer L, Herzele S, Zimmermann T, Saake B, Edler M, Grießer T, Konnerth J, Gindl-Altmutter W (2017) Reduced polarity and improved dispersion of microfibrillated cellulose in poly (lactic-acid) provided by residual lignin and hemicellulose. J Mater Sci 52:60–72

35. Nair SS, Kuo P-Y, Chen H, Yan N (2017) Investigating the effect of lignin on the mechanical, thermal, and barrier properties of cellulose nanofibril reinforced epoxy composite. Ind Crops Prod 100:208–217

36. Razab MA, Ghani RM, Noor A, Mocktar N, Zin FM, Abdullah N, Yusuf NN, Mohamed M (2019) Kenaf cellulose nanofibrils as mechanical enhancers of composite brick. In: AIP Conference Proceedings, 2019. vol 1. AIP Publishing LLC, Melville, NY, USA, p 020071

37. Sundheq A, Sundherg K, Lillandt C, Holmhom B (1996) Determination of hemicelluloses and pectins in wood and pulp fibres by acid methanolysis and gas chromatography. Nord Pulp Pap Res J 11(4):216–219. https://doi.org/10.3183/npprj-1996-11-04-p216-219

38. TAPPI T, (2006) Acid-insoluble lignin in wood and pulp (Reaffirmation of T 222 om-02). TAPPI Stand 222:1–7

39. Seifert R, Gharehkhani S, Vargas Figueroa D, Mercuur J, Olson J (2023) Engineering the paper production by combined fiber fractionation and reinforcement with microfibrillated cellulose. Cellulose 30(5):3201–3217

40. Liu K, Du H, Zheng T, Liu W, Zhang M, Liu H, Zhang X, Si C (2021) Lignin-containing cellulose nanomaterials: preparation and applications. Green Chem 23(24):9723–9746

41. Yuan T, Zeng J, Wang B, Cheng Z, Chen K (2021) Lignin containing cellulose nanofibers (LCNFs): lignin content-morphology-rheology relationships. Carbohyd Polym 254:117441

42. Deng J, Sun S-F, Zhu E-Q, Yang J, Yang H-Y, Wang D-W, Ma M-G, Shi Z-J (2021) Sub-micro and nano-lignin materials: small size and rapid progress. Ind Crops Prod 164:113412

43. Lee S-H, Chang F, Inoue S, Endo T (2010) Increase in enzyme accessibility by generation of nanospace in cell wall supramolecular structure. Biores Technol 101(19):7218–7223

44. Martins CCN, Dias MC, Mendonça MC, Durães AFS, Silva LE, Félix JR, Damásio RAP, Tonoli GHD (2021) Optimizing cellulose microfibrillation with NaOH pretreatments for unbleached *Eucalyptus* pulp. Cellulose 28:11519–11531

45. Schwanninger M, Stefke B, Hinterstoisser B (2011) Qualitative assessment of acetylated wood with infrared spectroscopic methods. J Near Infrared Spectrosc 19(5):349–357. https://doi.org/10.1255/jnirs.942

46. Mohebby B (2008) Application of ATR infrared spectroscopy in wood acetylation. J Agric Sci Technol 10:253–259

47. Laine C, Harlin A, Hartman J, Hyvärinen S, Kammiovirta K, Krogerus B, Pajari H, Rautkoski H, Setälä H, Sievänen J, Uotila J, Vähä-Nissi M (2013) Hydroxyalkylated xylans—their synthesis and application in coatings for packaging and paper. Ind Crops Prod 44:692–704. https://doi.org/10.1016/j.indcrop.2012.08.033

48. Selamat ME, Hashim R, Sulaiman O, Kassim MHM, Saharudin NI, Taiwo OFA (2019) Comparative study of oil palm trunk and rice husk as fillers in gypsum composite for building material. Constr Build Mater 197:526–532

49. Wardani AK, Sutrisno A, Faida TN, Yustina RD, Murdiyatmo U (2021) Ethanol production from oil palm trunk: a combined strategy using an effective pretreatment and simultaneous saccharification and cofermentation. Int J Microbiol 2021:1–12

50. Modenbach A, Nokes ES (2014) Effects of sodium hydroxide pretreatment on structural components of biomass. Trans ASABE 57(4):1187–1198. https://doi.org/10.13031/trans.57.10046

51. Oh SY, Yoo DI, Shin Y, Kim HC, Kim HY, Chung YS, Park WH, Youk JH (2005) Crystalline structure analysis of cellulose treated with sodium hydroxide and carbon dioxide by means of X-ray diffraction and FT-IR spectroscopy. Carbohydr Res 340(15):2376–2391. https://doi.org/10.1016/j.carres.2005.08.007

52. Oudiani AE, Chaabouni Y, Msahli S, Sakli F (2011) Crystal transition from cellulose I to cellulose II in NaOH treated *Agave americana* L. fibre. Carbohydr Polym 86(3):1221–1229. https://doi.org/10.1016/j.carbpol.2011.06.037

53. Winter A, Mundigler N, Holzweber J, Veigel S, Müller U, Kovalcik A, Gindl-Altmutter W (2018) Residual wood polymers facilitate compounding of microfibrillated cellulose with poly(lactic acid) for 3D printer filaments. Philos Trans R Soc Mathe Phys Eng Sci 376:20170046. https://doi.org/10.1098/rsta.2017.0046

54. Herzele S, Veigel S, Liebner F, Zimmermann T, Gindl-Altmutter W (2016) Reinforcement of polycaprolactone with microfibrillated lignocellulose. Ind Crops Prod 93:302–308. https://doi.org/10.1016/j.indcrop.2015.12.051

55. Jonoobi M, Khazaeian A, Tahir PM, Azry SS, Oksman K (2011) Characteristics of cellulose nanofibers isolated from rubberwood and empty fruit bunches of oil palm using chemo-mechanical process. Cellulose 18(4):1085–1095. https://doi.org/10.1007/s10570-011-9546-7

56. Zaini LH, Jonoobi M, Tahir PM, Karimi S (2013) Isolation and characterization of cellulose whiskers from kenaf (*Hibiscus cannabinus* L.) bast fibers. J Biomater Nanobiotechnol 4:37–44

57. Chen W-H, Wang C-W, Ong HC, Show PL, Hsieh T-H (2019) Torrefaction, pyrolysis and two-stage thermodegradation of hemicellulose, cellulose and lignin. Fuel 258:116168

58. Jose C, George K (2015) Sisal nanofibril reinforced polypropylene/polystyrene blends: morphology, mechanical, dynamic mechanical and water transmission studies. Ind Crops Prod 71:173–184

59. Liu Y, Chen B, Lv Y, Ye X, Lin C, Liu M (2022) Insight into the performance of lignin-containing cellulose nanofibers (LCNFs) via lignin content regulation by *p*-toluenesulfonic acid delignification. Cellulose 29(4):2273–2287

60. Ma S, He F, Tian D, Zou D, Yan Z, Yang Y, Zhou T, Huang K, Shen H, Fang J (2018) Variations and determinants of carbon content in plants: a global synthesis. Biogeosciences 15(3):693–702

61. Osman NS, Sapawe N (2020) Preparation of amorphous oil palm frond ash (OPFA) via acid leaching treatment as precursor for silica synthesis. Mater Today Proc 31:253–256

62. Spitzmüller L, Nitschke F, Rudolph B, Berson J, Schimmel T, Kohl T (2023) Dissolution control and stability improvement of silica nanoparticles in aqueous media. J Nanopart Res 25(3):40

63. Moberg T, Sahlin K, Yao K, Geng S, Westman G, Zhou Q, Oksman K, Rigdahl M (2017) Rheological properties of nanocellulose suspensions: effects of fibril/particle dimensions and surface characteristics. Cellulose 24(6):2499–2510

64. Grüneberger F, Künniger T, Zimmermann T, Arnold M (2014) Rheology of nanofibrillated cellulose/acrylate systems for coating applications. Cellulose 21:1313–1326
65. Goulet MT (1989) The effect of pulping, bleaching, and refining operations on the electrokinetic properties of wood fiber fines. Georgia Institute of Technology
66. Bismarck A, Springer J, Mohanty A, Hinrichsen G, Khan M (2000) Characterization of several modified jute fibers using zeta-potential measurements. Colloid Polym Sci 278(3):229–235
67. Cheng Z, Li J, Wang B, Zeng J, Xu J, Zhu S, Duan C, Chen K (2022) Comparative study on properties of nanocellulose derived from sustainable biomass resources. Cellulose 29(13):7083–7098. https://doi.org/10.1007/s10570-022-04717-0
68. Samimi S, Maghsoudnia N, Eftekhari RB, Dorkoosh F (2019) Chapter 3—Lipid-based nanoparticles for drug delivery systems. In: Mohapatra SS, Ranjan S, Dasgupta N, Mishra RK, Thomas S (eds) Characterization and biology of nanomaterials for drug delivery. Elsevier, Amsterdam, pp 47–76. https://doi.org/10.1016/B978-0-12-814031-4.00003-9

Publisher's Note